

An individual-based predator-prey model for biological coevolution: Fluctuations, stability, and community structure

Per Arne Rikvold^{1,2*}

¹*School of Computational Science,
Center for Materials Research and Technology,
and Department of Physics, Florida State University,
Tallahassee, Florida 32306-4120, USA*

²*National High Magnetic Field Laboratory,
Tallahassee, Florida, 32310-3706, USA*

(Dated: December 21, 2018)

We study an individual-based predator-prey model of biological coevolution, using linear stability analysis and large-scale kinetic Monte Carlo simulations. The model exhibits approximate $1/f$ noise in diversity and population-size fluctuations, and it generates a sequence of quasi-steady communities in the form of simple food webs. These communities are quite resilient toward the loss of one or a few species, which is reflected in different power-law exponents for the durations of communities and the lifetimes of species. The exponent for the former is near -1 , while the latter is close to -2 .

PACS numbers: 87.23.Kg 05.40.-a 05.65.+b

I. INTRODUCTION

Biological evolution presents many problems concerning interacting multi-entity systems far from equilibrium that are well suited for methods from nonequilibrium statistical physics [1, 2]. Among these are questions concerning the dynamics of the emergence and extinction of species on macroevolutionary timescales [3, 4, 5]. Traditionally it has been common to treat ecological and evolutionary processes on very different timescales. However, it has recently been realized that evolution often can take place on short timescales, comparable to those of ecological processes [6, 7, 8, 9]. A well-known example of very rapid evolution is provided by the cichlid fishes of East Africa [10]. Several models have therefore been proposed that, while spanning disparate scales of temporal and taxonomic resolution, consider the complex problem of coevolution of species in a fitness landscape that constantly changes with the composition of the community. Early contributions were simulations of allopatric speciation [11] and the coupled NK model with population dynamics [12, 13]. More recent work includes the Webworld model [8, 14, 15], the tangled-nature model [16, 17, 18] and simplified versions of the latter [19, 20, 21], as well as network models [22, 23]. Recently, large individual-based simulations have also been performed of parapatric and sympatric speciation [24, 25] and of adaptive radiation [26].

Many of the models discussed above are deliberately quite simple, aiming to elucidate universal features that are largely independent of the finer details of the ecological interactions and the evolutionary mechanisms. Such features may include lifetime distributions for species and communities, as well as other aspects of extinction statistics, statistical properties of fluctuations in diversity and population sizes, and the structure and dynamics of food webs that develop and change with time.

In the present paper we continue our study of a simplified version of the tangled-nature model. In the early studies of this individual-based model of coevolution [19, 20, 21], the interspecies interactions, which are described by an interaction matrix \mathbf{M} [27], were random and could produce any combination of pair interactions: favorable-favorable, deleterious-deleterious, or favorable-deleterious. Under those conditions the model was found to evolve through a sequence of quasi-stable communities, in which all species interact with mutually favorable interactions, i.e., mutualistic or symbiotic communities. For that reason we shall hereafter refer to that version of the model as *the mutualistic model*. Here we instead concentrate on a version that specifically describes the evolution of predator-prey communities. This restriction is enforced by means of an antisymmetric interaction matrix, so that an interaction that is favorable for one member of a pair is deleterious for the other, or *vice versa*. Many aspects of the dynamics of this predator-prey model are similar to the mutualistic model, such as approximate $1/f$ noise in species diversity and population sizes, and power-law distributions of the durations of communities and the lifetimes of species. However,

*Electronic address: rikvold@scs.fsu.edu

some of the power-law exponents are different, and, most importantly, the predator-prey model produces communities that take the form of simple food webs. It also shares with the mutualistic model the property that mean population sizes and stability properties of fixed-point communities can be calculated exactly in the absence of mutations. Comparisons of some aspects of the predator-prey model (with a much smaller number of potential species than used here) to those of the mutualistic model have been presented in Refs. [28, 29]. The focus of the present paper is a much more detailed discussion of the dynamics and the structure of the resulting food webs for the predator-prey model with a large number of potential species. For this purpose we use both exact linear-stability analysis and large-scale kinetic Monte Carlo simulations. In particular we wish to study the fluctuations in the statistically stationary state that develops for long times. A motivation is the hope that understanding of these stationary-state fluctuations can provide information about the system’s sensitivity to external perturbations in a way analogous to a fluctuation-dissipation relation [30]. We therefore carry out very long simulations.

The rest of this paper is organized as follows. The model is presented in Sec. II. Exact linear-stability analysis is performed in Sec. III, including fixed-point population sizes in Sec. III A and stability considerations in Sec. III B. Numerical results are presented in Sec. IV, including time series of diversities and population sizes (Sec. IV A), power spectral densities (Sec. IV B), durations of evolutionarily quiet and active periods (Sec. IV C), species lifetimes (Sec. IV D), and community structure and stability (Sec. IV E). Our conclusions are summarized in Sec. V, and the method used to calculate the interaction matrices for systems with a large number of potential species is explained in Appendix A.

II. MODEL

The model considered here is a version of the macroevolution model introduced by Rikvold and Zia [19] as a simplification of the tangled-nature model of Jensen and coworkers [16, 17, 18]. In this version, the interspecies interactions are constrained to represent a pure predator-prey system. As in Ref. [19], selection is provided by the reproduction rates in an individual-based, simplified multispecies population-dynamics model with nonoverlapping generations. This interacting birth/death process is augmented to enable evolution of new species by a mutation mechanism. The mutations act on a haploid, binary “genome” of length L , as introduced by Eigen for molecular evolution [31, 32]. This bit string defines the species, which are identified by the integer label $I \in [0, 2^L - 1]$. Typically, only a few of these 2^L potential species are resident in the community at any one time.

During reproduction, an offspring individual may undergo a mutation that flips a randomly chosen gene ($0 \rightarrow 1$ or $1 \rightarrow 0$) with a small probability, μ . The mutation thus corresponds to diffusional moves from corner to corner along the edges of an L -dimensional hypercube [33, 34]. A mutated individual is assumed to belong to a different species than its parent, with different properties. Genotype and phenotype are thus in one-to-one correspondence in this model. This is clearly a highly idealized picture, and it is introduced to maximize the pool of different species available within the computational resources. The approximation is justified by a large-scale computational study of the version of the model studied in Ref. [19], in which species that differ by as many as $L/2$ bits have correlated properties [21]. Remarkably, this study reveals that the more realistic, correlated model has long-time dynamical properties very similar to the uncorrelated model.

The reproduction probability $P_I(t)$ for an individual of species I in generation t depends on the individual’s ability to utilize the amount R of available external resources, and on its interactions with the population sizes $n_J(t)$ of all the species present in the community at that time. The dependence of P_I on the set of n_J is determined by an *interaction matrix* \mathbf{M} [27] with elements $M_{IJ} \in [-1, 1]$ in a way defined specifically in the next paragraph. The elements of \mathbf{M} are chosen randomly at the beginning of each simulation run and are subsequently kept constant throughout the run (quenched randomness). [For a discussion of how the matrix elements are created for $L > 13$, in which case the $2^L \times 2^L$ matrix does not fit into the memory of a standard workstation, see Appendix A.] In contrast to our previously studied model [19, 20, 21], in which the interaction matrix has no particular structure, the predator-prey dynamics is enforced by the requirement that the off-diagonal part of \mathbf{M} must be antisymmetric. Thus, if $M_{IJ} > 0$ and $M_{JI} < 0$, then species I is the predator and J the prey, and *vice versa*.

Specifically, the reproduction probability for species I , $P_I(t)$, depends on R and the set $\{n_J(t)\}$ through the nonlinear form,

$$P_I(t) = \frac{1}{1 + \exp[-\Delta_I(R, \{n_J(t)\})]}, \quad (1)$$

where

$$\Delta_I(R, \{n_J(t)\}) = -b_I + \eta_I R/N_{\text{tot}} + \sum_J M_{IJ} n_J(t)/N_{\text{tot}}. \quad (2)$$

Here b_I is the “cost” of reproduction for species I (always positive), and η_I (positive for primary producers or autotrophs, and zero for consumers or heterotrophs) is the ability of individuals of species I to utilize the external resource R . The latter is renewed at the same level every generation and does *not* have independent dynamics. The total population size is $N_{\text{tot}}(t) = \sum_J n_J(t)$. [In contrast, the total number of *species* present in generation t (the species richness) will be defined as $\mathcal{N}(t)$.] For large positive Δ_I , (small birth cost, strong coupling to the external resources, and more prey than predators), the individual almost certainly reproduces, giving rise to F offspring. In the opposite limit of large negative Δ_I , (large birth cost, weak or no coupling to the external resources, and/or more predators than prey), it almost certainly dies without offspring. The nonlinear dependence of P_I on Δ_I thus limits the growth rate of the population size, even under extremely favorable conditions. It also sets a practical negative limit on Δ_I , below which conditions are so unfavorable that reproduction is virtually impossible. (A more general version of Eq. (2), in which population growth is limited by a “Verhulst factor” [35] or “environmental carrying capacity” [36] as is necessary in models that allow mutualistic interactions, is discussed in Ref. [29].)

The normalization of Δ_I with N_{tot} implies global competition. This is not very realistic, but it enables us to find exact expressions for the stationary values of the average population sizes in the mutation-free limit. (See Sec. III A.) The model can thus be used as a benchmark for more realistic ones in future research.

An analytic approximation describing the development in time of the mean population sizes (averaged over independent realizations), $\langle n_I(t) \rangle$, can be written as a set of coupled difference equations,

$$\begin{aligned} \langle n_I(t+1) \rangle &= \langle n_I(t) \rangle F P_I(R, \{ \langle n_J(t) \rangle \}) [1 - \mu] \\ &+ (\mu/L) F \sum_{K(I)} \langle n_{K(I)}(t) \rangle P_{K(I)}(R, \{ \langle n_J(t) \rangle \}) , \end{aligned} \quad (3)$$

where $K(I)$ is the set of species that can be generated from species I by a single mutation (“nearest neighbors” of I in genotype space).

III. LINEAR STABILITY ANALYSIS

A. Fixed-point communities

An advantage of the model studied here is that its fixed-point communities in the mutation-free limit can be found exactly within a mean-field approximation based on Eq. (3) [19]. To obtain a stationary solution for a community of \mathcal{N} species, we must require $P_I = 1/F$ for all \mathcal{N} species. Equations (1) and (2) then give rise to \mathcal{N} linear relations, which can be written on the matrix form

$$-|\tilde{b}\rangle N_{\text{tot}}^* + |\eta\rangle R + \hat{\mathbf{M}}|n^*\rangle = 0 , \quad (4)$$

where $\tilde{b}_I = b_I - \ln(F-1)$, $|\tilde{b}\rangle$, $|\eta\rangle$, and $|n^*\rangle$ are the column vectors of \tilde{b}_I , η_I , and n_I^* , respectively (in all cases including only those \mathcal{N} species that have nonzero n_I^*), and $\hat{\mathbf{M}}$ is the corresponding $\mathcal{N} \times \mathcal{N}$ submatrix of \mathbf{M} . (For simplicity, we drop the $\langle \rangle$ notation for the average population sizes, and the asterisk superscripts denote fixed-point solutions.)

The solution for $|n^*\rangle$ is

$$|n^*\rangle = -\hat{\mathbf{M}}^{-1} \left[|\eta\rangle R - |\tilde{b}\rangle N_{\text{tot}}^* \right] , \quad (5)$$

where $\hat{\mathbf{M}}^{-1}$ is the inverse of $\hat{\mathbf{M}}$. To find each n_I^* , we must first obtain $N_{\text{tot}}^* \equiv \langle 1|n^*\rangle$, where $\langle 1|$ is an \mathcal{N} -dimensional row vector composed entirely of ones. Multiplying Eq. (5) from the left by $\langle 1|$, we obtain

$$R\mathcal{E} + \Theta N_{\text{tot}}^* = 0 , \quad (6)$$

where the coefficients

$$\Theta = \frac{1 - \langle 1|\hat{\mathbf{M}}^{-1}|\tilde{b}\rangle}{\langle 1|\hat{\mathbf{M}}^{-1}|1\rangle} \quad \text{and} \quad \mathcal{E} = \frac{\langle 1|\hat{\mathbf{M}}^{-1}|\eta\rangle}{\langle 1|\hat{\mathbf{M}}^{-1}|1\rangle} \quad (7)$$

have been written with $\langle 1|\hat{\mathbf{M}}^{-1}|1\rangle$ in the denominators in order to remain finite even for near-singular \mathbf{M} [29]. They can be viewed as an effective interaction strength and an effective coupling to the external resource, respectively. The solution of Eq. (6) is

$$N_{\text{tot}}^* = -\frac{R\mathcal{E}}{\Theta} = \frac{R\langle 1|\hat{\mathbf{M}}^{-1}|\eta\rangle}{\langle 1|\hat{\mathbf{M}}^{-1}|\tilde{b}\rangle - 1} . \quad (8)$$

To find each n_I^* separately, we now only need to insert this solution for N_{tot}^* in Eq. (5).

Only those $|n^*\rangle$ that have all positive elements can represent a *feasible* community [37]. If $\hat{\mathbf{M}} = \mathbf{0}$ or is otherwise singular, the set of equations (4) is inconsistent for $\mathcal{N} > 1$, unless \tilde{b}_I and η_I both are independent of I (this case is equivalent to $\mathcal{N} = 1$). The only possible stationary community then consists of one single species, the one with the largest value of η_I/\tilde{b}_I . This is a trivial example of competitive exclusion [38, 39, 40]. If η_I/\tilde{b}_I has the same value for all \mathcal{N} values of I , we have an example of a neutral model [41].

In Ref. [29] it was shown that Eq. (6) for fixed \mathcal{E} and Θ can be seen as a maximization condition for a “community fitness” function,

$$\Phi(N_{\text{tot}}) = \left(1 - \frac{1}{F}\right) \left(R\mathcal{E}N_{\text{tot}} + \frac{\Theta}{2}N_{\text{tot}}^2\right). \quad (9)$$

This result would not be particularly remarkable if \mathcal{E} and Θ were externally fixed parameters. However, extinctions and mutations provide a mechanism for both parameters to change as old species go extinct and new species emerge. In our numerical simulations we find that their values evolve toward and then fluctuate around values that maximize Φ , limited only by the internal constraints on \mathbf{M} and $|\tilde{b}_I\rangle$. In particular, this means that Θ approaches closely to 0 from the negative side [29]. In the simulations presented in this paper (see Sec. IV) we find that near the end of very long simulations, $\Theta \approx -0.10 \pm 0.03$ and $\mathcal{E} \approx 0.7 \pm 0.2$, corresponding to $N_{\text{tot}}^* \approx (7.4 \pm 1.4)R$.

B. Stability of fixed-point communities

The internal stability of an \mathcal{N} -species fixed-point community is obtained from the matrix of partial derivatives,

$$\left.\frac{\partial n_I(t+1)}{\partial n_J(t)}\right|_{|n^*\rangle} = \delta_{IJ} + \Lambda_{IJ}, \quad (10)$$

where δ_{IJ} is the Kronecker delta function and Λ_{IJ} are elements of the *community matrix* $\mathbf{\Lambda}$ [36]. Straightforward differentiation yields [29]

$$\Lambda_{IJ} = \left(1 - \frac{1}{F}\right) \frac{n_I^*}{N_{\text{tot}}^*} \left[M_{IJ} - \frac{R\eta_I + (\hat{\mathbf{M}}|n^*\rangle)_I}{N_{\text{tot}}^*} \right], \quad (11)$$

where $(\hat{\mathbf{M}}|n^*\rangle)_I$ is the element of the column vector $\hat{\mathbf{M}}|n^*\rangle$, corresponding to species I . In order for deviations from the fixed point to decay monotonically in magnitude, the magnitudes of the eigenvalues of the matrix of partial derivatives in Eq. (10), $\mathbf{\Lambda} + \mathbf{1}$, where $\mathbf{1}$ is the \mathcal{N} -dimensional unit matrix, must be less than unity. The value of the fecundity used in this work, $F = 2$, was chosen to satisfy this requirement for $\mathcal{N} = 1$.

Since new species are created by mutations, we must also study the stability of the fixed-point community toward “invaders.” Consider a mutant invader i . Then its multiplication rate, in the limit that $n_i \ll n_J$ for all \mathcal{N} species J in the resident community, is given by

$$\frac{n_i(t+1)}{n_i(t)} = \frac{F}{1 + \exp[-\Delta_i(R, \{n_J^*\})]}. \quad (12)$$

The Lyapunov exponent, $\ln[n_i(t+1)/n_i(t)]$, is the *invasion fitness* of the mutant with respect to the resident community [42, 43]. It will be studied numerically in Sec. IV E.

IV. NUMERICAL RESULTS

We performed twelve independent, long simulation runs of $2^{25} = 33\,554\,432$ generations of the model with the following parameters: genome length $L = 20$ (1 048 576 potential species), external resource $R = 2000$, and mutation rate $\mu = 10^{-3}$. These parameters were chosen to represent the realistic situation that the number of species resident in the community at any time is much smaller than the number of potential species (i.e., that $\mathcal{N}(t) \ll 2^L$), and also that $\mathcal{N}(t) \ll N_{\text{tot}}(t)$. In this parameter range the model is not very sensitive to the exact parameter values [29]. The very long simulation times were chosen because our main interest is in the stationary dynamics of macroevolution over timescales much longer than the ecological ones of a few generations. Each run therefore starts with a “warm-up period” of about one million generations before the 2^{25} -generation data-taking period. Details of the simulation algorithm were given in Ref. [19].

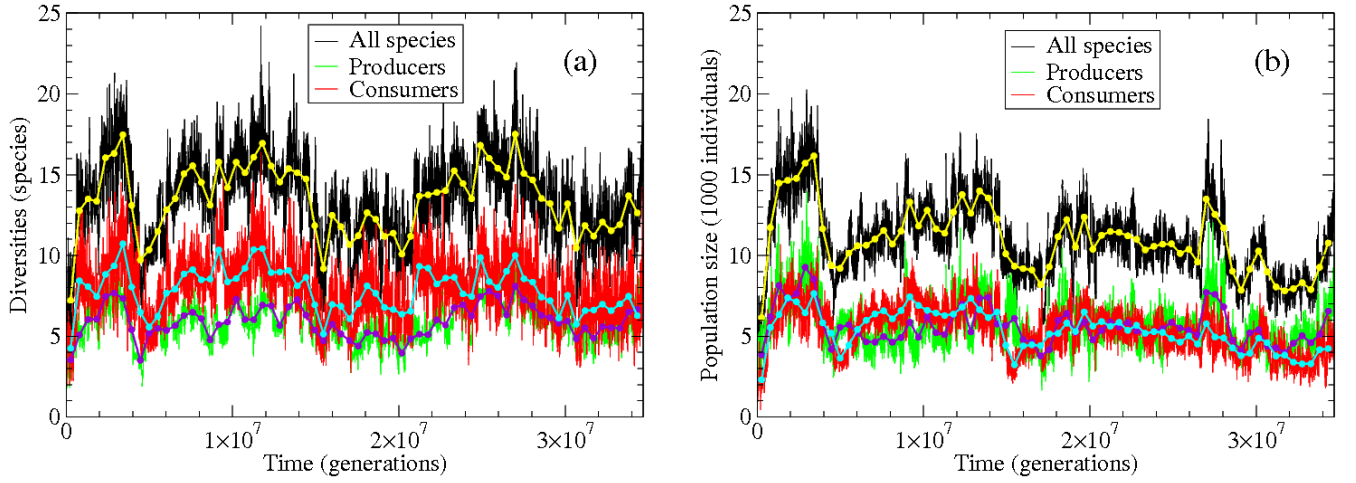


FIG. 1: (Color online.) Time series for the Shannon-Wiener diversity index (a) and the population sizes (b). The jagged curves in the background show data sampled every 2048 generations to show the rapid fluctuations, while the curves in contrasting color/brightness in the foreground are running averages over 524 288 generations, emphasizing the slower fluctuations. The three sets of curves represent all species (black/light gray; black/yellow online), producer species (light gray/dark gray; green/violet online), and consumer species (medium gray/light gray; red/cyan online).

A. Time series

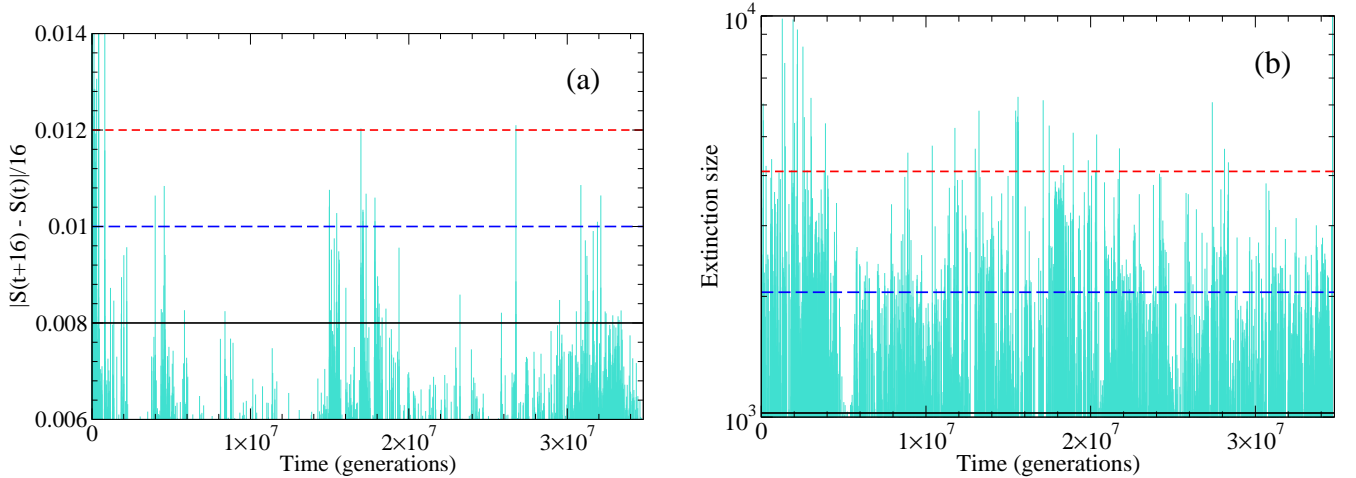


FIG. 2: (Color online.) Time series for the same simulation run shown in Fig. 1, displaying quantities that measure the evolutionary activity: the magnitude of the logarithmic derivative of the Shannon-Wiener diversity index, $|dS/dt|$ (averaged over 16 generations) (a), and the size of extinctions per generation (b). The horizontal lines in each part indicate cutoff levels used to define quiet and active periods as discussed in the text.

We collected time series of a number of quantities including several measures of diversity or species richness, as well as population sizes of producer and consumer species.

Time series of diversities and population sizes for one representative run are shown in Fig. 1. In order to filter out noise from the small-population species that are mostly unsuccessful mutations, we use the diversity measure known in ecology as the exponential Shannon-Wiener index [44]. It is defined as the exponential function of the information-theoretical entropy of the population distributions, $D(t) = \exp[S(\{n_I(t)\})]$, where

$$S(\{n_I(t)\}) = - \sum_{\{I|\rho_I(t)>0\}} \rho_I(t) \ln \rho_I(t) \quad (13)$$

with $\rho_I(t) = n_I(t)/N_{\text{tot}}(t)$ for the case of the curves labeled “All species” in Fig. 1. For the producers or consumers, the sums and normalization constant include only the appropriate species.

Time series of additional quantities that indicate the level of evolutionary activity are shown in Fig. 2 for the same simulation run as in Fig. 1. These are the magnitude of the logarithmic derivative of the Shannon-Wiener diversity index (Fig. 2(a)), and the size of extinctions per generation (Fig. 2(b)). The latter is defined as the sum of the maximum population sizes reached by the species that go extinct in each generation.

The properties of the fluctuations in the time series were analyzed with several methods, including power spectral densities (PSD), lifetimes of individual species, and the durations of quiet and active periods during the evolution. The results of each are reported in the following subsections.

B. Power spectral densities

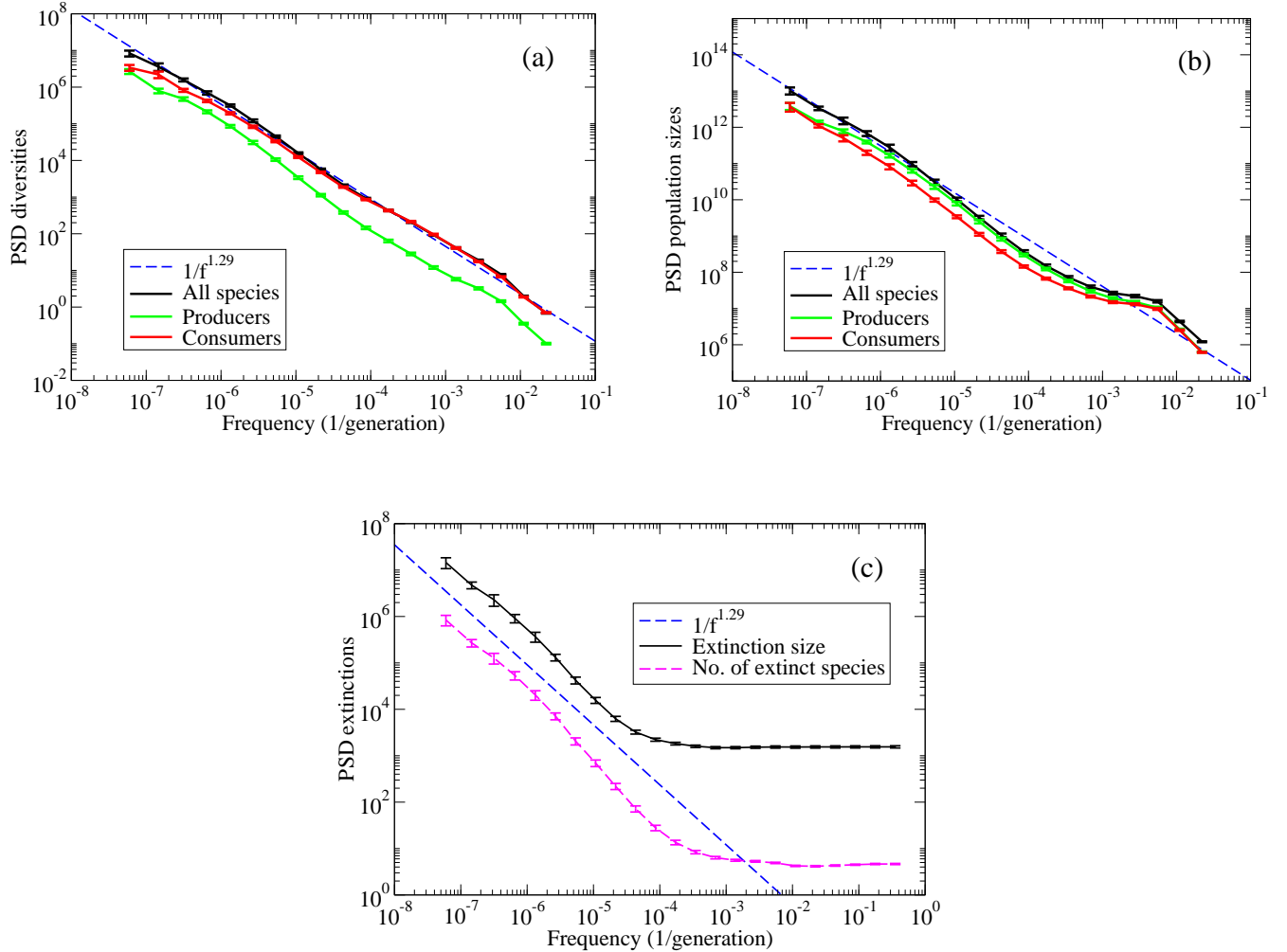


FIG. 3: (Color online.) PSDs for the diversities (a), population sizes (b), and the extinction sizes and number of species going extinct per generation (c), all averaged over twelve independent runs of 2^{25} generations. The error bars are estimated from the variations between the individual runs. The dashed straight line with slope -1.29 in (a) is a weighted fit to the PSD for the overall diversity over the whole frequency range. The dashed lines in (b) and (c) are guides to the eye with the same slope.

PSDs of the diversity and population-size fluctuations, averaged over the twelve independent simulation runs, are shown in Fig. 3, both for the total population and for the producers and consumers separately. The spectra indicate $1/f$ like noise over more than five decades in time. A weighted fit to the PSD for the overall diversity in Fig. 3(a) yields a power law $f^{-\alpha}$ with $\alpha \approx 1.29 \pm 0.01$. This power is also seen to fit reasonably well, both with the data for the diversities of producers and consumers over the whole frequency range in Fig. 3(a), and with the PSDs of all

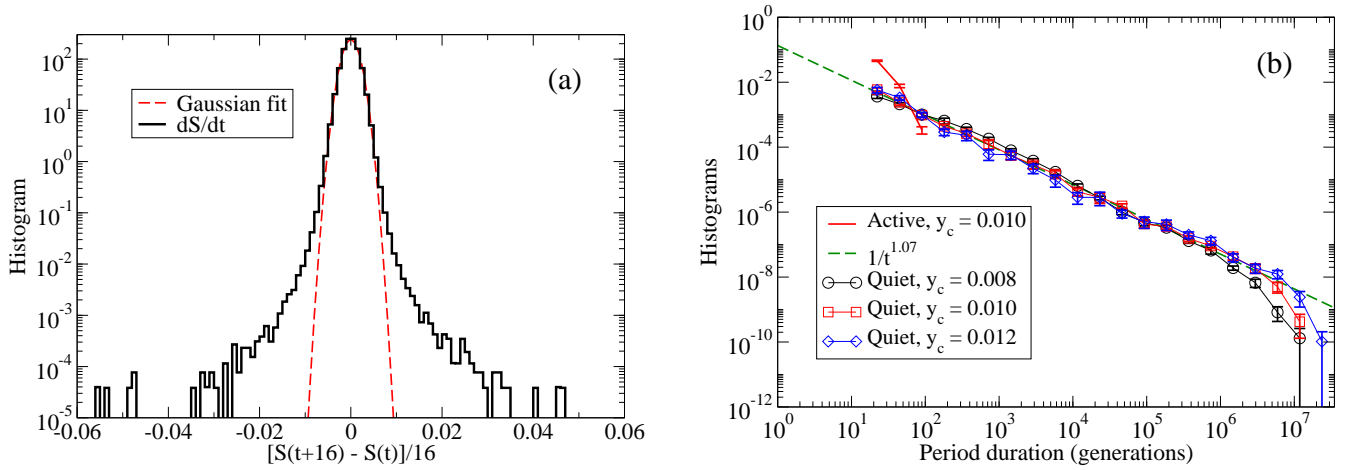


FIG. 4: **(a)** Histogram of the logarithmic derivative of the overall diversity, dS/dt . The data were averaged over 16 generations for each run and then over 12 independent runs. The dashed curve is a Gaussian fit. The time series of the magnitude of this quantity for one particular simulation run is shown in Fig. 2(a). **(b)** Histograms of the durations of active and quiet periods for various values of the cutoff y_c for $|dS/dt|$, averaged over 12 independent runs. The dashed, straight line with slope -1.07 is a weighted fit to the histogram for the quiet periods for $y_c = 0.010$ between 10 and 10^6 generations. The steep histogram curve with only three data points between 10 and 100 generations corresponds to the active periods, which are always very short.

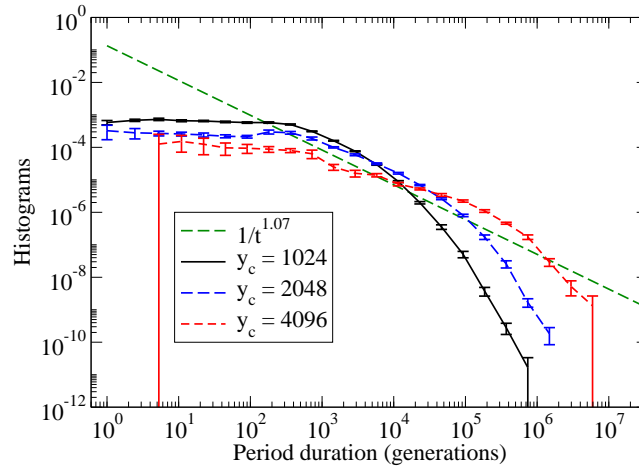


FIG. 5: Histograms of the durations of quiet periods, obtained from the time series of extinction sizes, an example of which is shown in Fig. 2(b). Data averaged over 12 independent simulation runs. The straight, dashed line with slope -1.07 is a guide to the eye, based on the fit to the QSS duration distribution based on $|dS/dt|$, shown in Fig. 4(b).

three population measures at low frequencies in Fig. 3(b), as well as for the extinction measures at low frequencies in Fig. 3(c). This suggests that the long-time fluctuations in the diversity, as well as in the population sizes and the extinction measures, obey the same power law on long timescales. On short timescales the PSDs for the population sizes have a more complicated structure, possibly indicating overdamped oscillations on a scale of a few hundred generations. The extinction measures show a wide region of white noise for high frequencies, due to the frequent extinction of unsuccessful mutants. However, the behaviors for low frequencies appear consistent with the diversities and the population sizes.

C. Quiet and active periods

From the time series shown in Figs. 1 and 2 one sees that periods of moderate fluctuations are punctuated by periods of high activity. The communities corresponding to the lower fluctuation levels are known as quasi-static states (QSS) and correspond to the fixed-point communities of the mutation-free system [19, 20]. One measure of the degree of activity is the time derivative of the entropy or, equivalently, the logarithmic derivative of the total diversity. Its magnitude is shown as a time series in Fig. 2(a), and a histogram is shown in Fig. 4(a). While the central part of the distribution is well approximated by a Gaussian, the wings are heavy – possibly exponential or even power-law. Quiet and active periods were defined as contiguous periods during which $|dS/dt|$ stayed below or above a cutoff y_c , respectively. Octave-binned histograms for the probability distributions of the durations of quiet and active periods are shown in Fig. 4(b) for various cutoffs. For the quiet periods a power law is seen with exponent near -1 (a weighted fit between 10 and 10^6 generations gives $t^{-\tau}$ with $\tau \approx 1.07 \pm 0.01$) and a long-time cutoff that increases with increasing y_c . The active periods for all values of y_c are very brief in comparison. (Their histogram for $y_c = 0.010$ is the steep curve with only three data points between 10 and 100 generations in Fig. 4(b).) As a consequence, the system spends most of its time in QSS communities – a situation consistent on the community level with Eldredge and Gould’s concept of punctuated equilibria [45, 46, 47].

Durations of quiet periods could also be obtained from the time series of extinction sizes in Fig. 2(b). Due to the white noise at short timescales, which was also apparent in the PSDs in Fig. 3(c), the power-law behavior is limited to a window of longer times between about 1000 generations and the strongly cutoff-dependent long-time decay. As a result, this quantity does not provide as clear a quiet-period distribution as the entropy derivative. We therefore did not perform any independent fit to obtain a power-law exponent for the QSS durations measured this way. See Fig. 5. The decay with time is qualitatively consistent with that observed in Fig. 4(b) for the QSS duration distributions based on $|dS/dt|$.

D. Species lifetimes

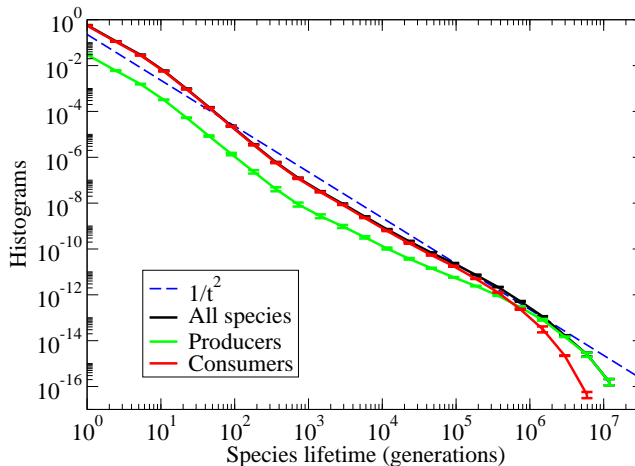


FIG. 6: (Color online.) Histograms for the lifetimes of individual species. The dashed, straight line is a guide to the eye, corresponding to a t^{-2} power law. Data averaged over 12 independent simulation runs.

Another set of times that are characteristic of the evolution process, are the lifetimes of individual species. The species lifetime is defined as the time from a particular species enters the community, till it goes extinct (i.e., its first return time to zero population size). Histograms showing the distributions of species lifetimes, for all species as well as for producers and consumers separately, are shown in Fig. 6. Although there are some undulations in these curves, they remain close to a power law $t^{-\tau_1}$ with exponent $\tau_1 \approx 2$ over more than six decades in time, which is the maximum we could expect with the length of our simulations.

Lifetime distributions for marine genera that are compatible with a power law exponent in the range -1.5 to -2.5 have been obtained from the fossil record [3, 4, 5]. However, the possible power-law behavior in the fossil record is only observed over about one decade in time – between 10 and 100 million years – and other fitting functions, such as exponential or log-normal, are also possible. Nevertheless, it is reasonable to conclude that the numerical

results obtained from complex, interacting evolution models that extend over a large range of time scales support interpretations of the fossil lifetime evidence in terms of nontrivial power laws.

It is quite remarkable that the exponent for the species lifetimes is significantly different from the one for the QSS duration, which is close to unity. This is particularly so because the two exponents appear to be the same for the mutualistic version of the model [19]. We believe that the explanation lies in the structure of the QSS communities generated by the present evolution process, which take the form of simple food webs. These will be studied in Sec. IV E below.

E. QSS community structure and stability

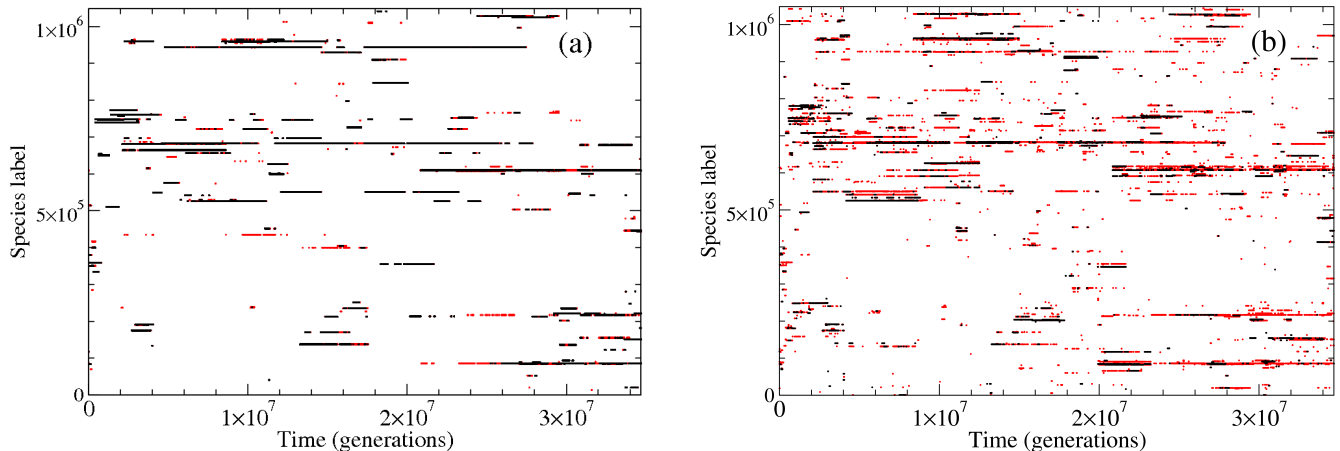


FIG. 7: (Color online.) Major populated species shown vs time for the same simulation run shown in Figs. 1 and 2. The horizontal lines correspond to the species label, and the grayscales (color online) to the population size. Black: $n_I > 1000$. Gray (red online): $n_I \in [101, 1000]$. (a): Producers. (b): Consumers.

The evolution process in the present model generates dynamic communities, in which species emerge, exist for a shorter or longer time, and eventually go extinct. The emergence and extinction of a major species are quite fast processes on the evolutionary timescale, and so the vast majority of randomly selected communities are QSS communities. This is confirmed by the short durations of evolutionarily active periods, shown by the corresponding histogram in Fig. 4(b). Diagrams of the population sizes of major producer and consumer species as functions of time in a particular simulation run are shown in Figs. 7(a) and (b), respectively. In these figures a horizontal line represents a species. The beginning of the line represents the emergence of the species, and the end represents its extinction. The population size is represented by the color of the line. We see that some species persist for tens of millions of generations, while others are so short-lived as to hardly be visible on the scale of these figures. This is consistent with the power-law behavior of the species-lifetime distribution (see Fig. 6). We also see that producer species appear to emerge and go extinct relatively independently of each other, while there is a significant correlation between the producer and consumer species. The structure of these plots contrasts with that of similar plots for the mutualistic model of Ref. [19] (see Fig. 2 of that paper), in which species tend to emerge as well as go extinct together. We believe this is the reason for the decoupling of the exponents for the species lifetimes and the durations of QSS communities in this model: the overall community is relatively resilient toward losing or gaining a single species. As a community it is more long-lived than the individual species, leading to the smaller value for the exponent of the distribution for the QSS durations (compare Figs. 4(b) and 6). (A similar relationship has been noted between the lifetimes of orders and their constituent genera in the fossil record [5].)

Three representative QSS communities from the same simulation run shown in Figs. 1, 2, and 7 are shown in Fig. 8. These are consecutive communities near 22×10^6 , 27×10^6 , and 34×10^6 generations, respectively. They are all stable by the eigenvalue criterion discussed in Sec. III B. The communities take the form of simple food webs with two trophic levels above the resource node. Communities with three trophic levels are also occasionally observed. The different branches of the webs are relatively independent of each other, and many consumer species have more than one prey. Both features contribute to the resilience against mass extinctions discussed above.

The relative stability of evolved QSS communities with respect to invasion by mutants is illustrated in Fig. 9. The results are averaged over 14 QSS communities – the three shown in Fig. 8 plus the final communities of the eleven other

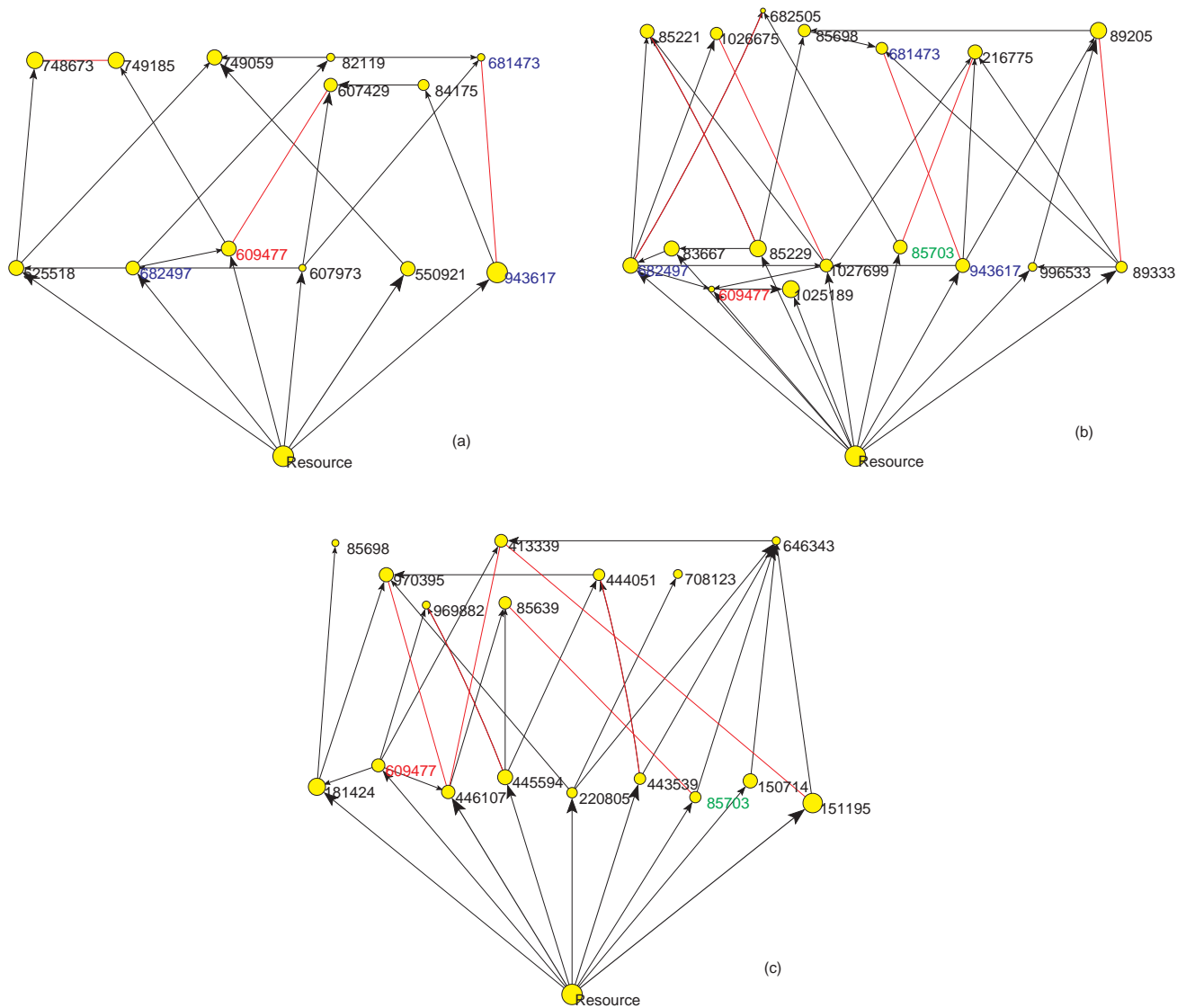


FIG. 8: (Color online.) Food webs for the simulation shown in Figs. 1, 2, and 7 at times near 22×10^6 generations (a), near 27×10^6 generations (b), and at the end of the simulation near 35×10^6 generations (c). The thickness and head size of the arrows correspond to the magnitude of M_{IJ} , and the area of the circles to the stationary population size, as calculated analytically from Eq. (5). Light gray (red online) lines connect nearest neighbors in genotype space. Labels in red mark species that persist from the first to the last snapshot, (a) to (c), while blue labels mark species that persist from (a) to (b), and green labels mark species that persist from (b) to (c). Black labels indicate species that are unique to the particular snapshot.

simulation runs. This figure shows the multiplication ratio of a small population of invaders (the exponential function of the invasion fitness), given by Eq. (12). Only about 2.3% of species outside the communities have multiplication ratios larger than unity, and most of these lie between 1.0 and 1.1. This percentage does not seem to depend significantly on the Hamming distance of the invader from the community. We also tested if the evolved QSS communities are more resilient toward invasion than randomly constructed feasible communities. Such communities are more difficult to construct in this model, than in the mutualistic model [19]. To have the same level of statistics as for the QSS communities, we produced 14 such communities in the following way. We started a run with a random sample of 200 species, each with $n_I = 10$, and evolved the community for 1024 generations *without* mutations. We then tested the remaining community for feasibility and removed species with a negative stationary population according to Eq. (5). The resulting feasible communities had much smaller diversity than the evolved QSS communities – an average of only 3.6 species per community. These communities had a significantly larger percentage of potential invaders – about

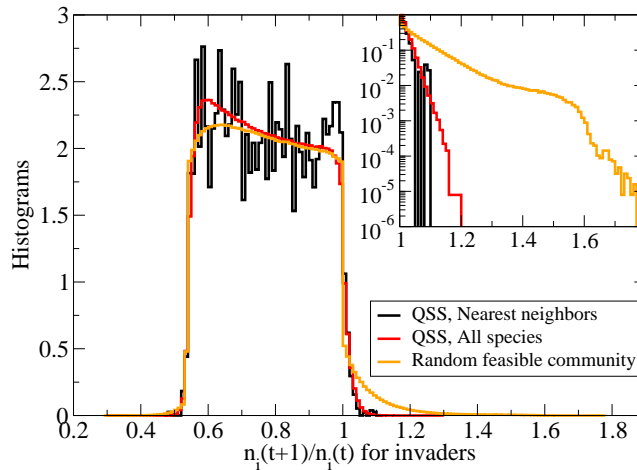


FIG. 9: (Color online.) Histograms of the multiplication ratio, $n_i(t+1)/n_i(t)$ (exponential of the invasion fitness, Eq. (12)) for low-density invaders. Each curve is averaged over 14 different communities. Black: nearest neighbors in genotype space against stable QSS communities. Dark gray (red online): All species not in the community against stable QSS communities. Light gray (orange online): All species not in the community against random feasible communities. Inset: The part of the distributions for potentially successful invaders, $n_i(t+1)/n_i(t) > 1$, with the y -axis on logarithmic scale. The tails appear nearly exponential.

4%, with a maximum multiplication ratio near 1.7 (see inset in Fig. 9). While there thus is a clear difference between the stability against invaders of QSS communities and random feasible communities, the difference is not as large as it is for the mutualistic model of Ref. [19]. (See Fig. 3 of that paper.)

V. SUMMARY AND CONCLUSIONS

In this paper we have studied in detail an individual-based predator-prey model of biological coevolution, based on the simplified version of the tangled-nature model [16, 17, 18] that was introduced in Ref. [19]. Selection is provided by a population-dynamics model in which the reproduction probability of an individual of a particular species depends nonlinearly on the amount of external resources and on the population densities of all other species resident in the community. New species appear in the community through point mutations in a genome consisting of a string of L bits.

In the mutation-free limit, the mean fixed-point population sizes and stability properties of any \mathcal{N} -species community can be obtained exactly by linear stability analysis. While the universal competition effect that enables this analytical treatment is not very realistic, the exact solutions make the model ideal as a benchmark for more realistic, but also more complicated, models. A preliminary discussion of two more realistic models is found in Ref. [48].

In the simulations presented here, we used $L = 20$ for a total of $2^{20} = 1\,048\,576$ potential species. In order to study the statistically stationary properties of the model, we performed long kinetic Monte Carlo simulations over $2^{25} = 33\,554\,432$ generations. By studying the stationary fluctuations we hope in the future to gain an understanding of the the system's sensitivity to external perturbations in a way analogous to the fluctuation-dissipation relations of equilibrium statistical mechanics [30].

Qualitatively, many of the statistical properties of this model are similar to those of the related, mutualistic model studied in Refs. [19, 20, 21]. These include approximate $1/f$ noise in power spectra (PSDs) of diversity and population sizes ($f^{-\alpha}$ with $\alpha \approx 1.29$), as well as power-law distributions for the lifetimes of individual species, as well as of the durations of evolutionarily quiet periods, corresponding to QSS communities. However, in contrast to the mutualistic model, the power-law exponents for the species lifetimes and QSS durations are different: $t^{-\tau_1}$ with $\tau_1 \approx 2$ for the former and $t^{-\tau}$ with $\tau \approx -1.07$ for the latter. In Ref. [28] it was speculated that the exponent values $\alpha = 1$, $\tau_1 = 2$, and $\tau = 1$ are consistent with predictions for a zero-dimensional extremal-dynamics model [49, 50]. However, this speculation is not consistent with the presumably more accurate estimate for α presented here, and it seems advisable to be rather skeptical about any mapping of the current model onto a simple statistical-mechanical extremal-dynamics model.

It is probably more fruitful to consider why τ_1 and τ are different for the current predator-prey model, while they

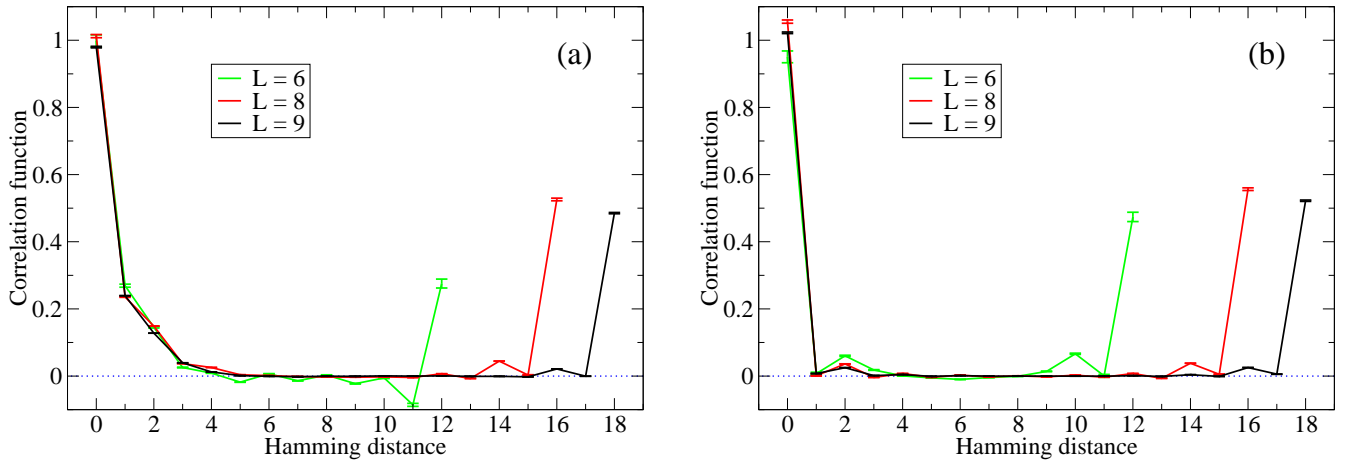


FIG. 10: (Color online.) Normalized correlation functions for the matrix elements M_{IJ} for the two schemes described in the text, each based on a single realization of \mathbf{M} for $L = 6, 8,$ and 9 . (a) The scheme described in Ref. [17]. (b) The modified scheme introduced here.

coincide for the corresponding mutualistic model. Here we believe the answer lies in the different community structures in the two models. While communities in the mutualistic model are tightly knit with all positive interactions (see Fig. 10 of Ref. [29]), the communities in the present predator-prey model take the form of food webs, which are much more resilient toward the loss of a single or a few species. In this sense, this predator-prey model is considerably more realistic than the mutualistic model. More detailed studies of the structure of the food webs generated by the model are planned.

Acknowledgments

The author thanks V. Sevim for useful discussions and for calculating the correlation functions shown in Fig. 10.

The research was supported in part by National Science Foundation Grant Nos. DMR-0240078 and DMR-0444051, and by Florida State University through the School of Computational Science, the Center for Materials Research and Technology, and the National High Magnetic Field Laboratory.

APPENDIX A: MATRIX ELEMENTS FOR LARGER GENOMES

Here we describe an improved version of the method introduced by Hall et al. [16, 17] to produce pseudorandom matrix elements M_{IJ} for values of L that are too large for the full $2^L \times 2^L$ matrix \mathbf{M} to fit into computer memory. This method permits the matrix elements for a given community to be generated and retained only as needed. We first present Hall et al.'s method, point out some problematic features, and then present our modifications.

Let $\mathbf{S}(I)$ be the string of binary digits corresponding to the decimal species label I . This bit string has length L , so there are 2^L different strings. To generate the matrix element M_{IJ} , one first generates a new string of the same length, $\mathbf{S}(I, J) = \mathbf{S}(I) \text{XOR} \mathbf{S}(J)$, where XOR is the logical *exclusive or* operator. From this bit string is generated the corresponding new decimal index $K(\mathbf{S}(I, J))$. Next one creates two one-dimensional arrays, \mathbf{X} and \mathbf{Y} , each of 2^L random numbers between -1 and $+1$. (For simplicity let the starting index for the arrays be zero.) Since $\mathbf{S}(I, J)$ is symmetric in I and J , asymmetric pseudorandom matrix elements are generated as

$$M_{IJ} = [\mathbf{X}(K(\mathbf{S}(I, J))) + \mathbf{Y}(J)] / 2. \quad (\text{A1})$$

(Hall et al. instead use the product of the two random numbers, which gives a pseudorandom number with a slightly different distribution.)

The problem with this method is that it produces strong correlations along the columns of \mathbf{M} since the second of the two random numbers that produce M_{IJ} is the same for all I at the same J . In Fig. 10(a) we show the resulting correlation function for this scheme as a function of the Hamming distance between the pairs of bit strings involved

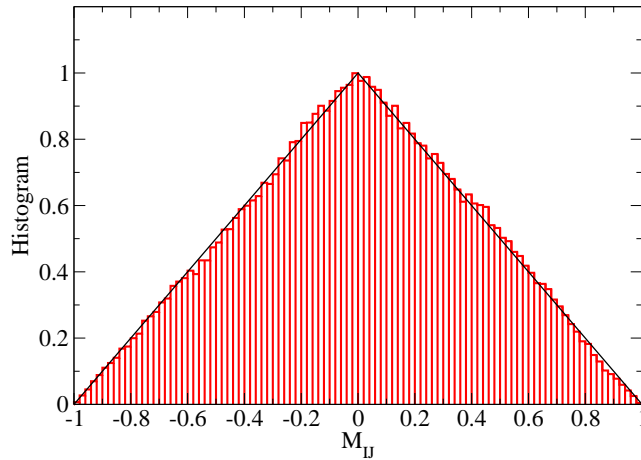


FIG. 11: (Color online.) Histogram for the pseudorandom M_{IJ} produced by the scheme introduced here for $L = 9$, corresponding to 262 144 individual matrix elements. The straight, black lines represent the triangular shape of the theoretical distribution.

in two different matrix elements. Regardless of L , significant correlations are seen for Hamming distances less than five. A discussion of how to calculate such correlation functions is found in Ref. [21].

To reduce these correlations between matrix elements involving closely related genotypes, we here modify the scheme as follows. We extend array \mathbf{Y} to a length of 3×2^L and define M_{IJ} as

$$M_{IJ} = [\mathbf{x}(K(\mathbf{S}(I, J))) + \mathbf{Y}(K(\mathbf{S}(I, J)) + 2(J + 1))] / 2. \quad (\text{A2})$$

The addition of $K(\mathbf{S}(I, J))$ in the index of \mathbf{Y} ensures that the matrix element depends in an erratic fashion on both I and J , while the term linear in J ensures that \mathbf{M} is not symmetric. The resulting correlation function is shown in Fig. 10(b). The correlations for elements involving closely related genotypes are strongly suppressed. The correlations for a Hamming distance of $2L$, which are present in both schemes, are of little practical significance. They are caused by the fact that the XOR operation is invariant under simultaneous bit reversal in both its arguments and could be removed by adding a linear function of I in the argument of \mathbf{x} . The probability density for M_{IJ} is triangular as expected from simple analytical arguments, and the whole interval from -1 to $+1$ is well sampled, even for relatively small L . This is shown in Fig. 11.

-
- [1] E. Baake and W. Gabriel, in *Annual Reviews of Computational Physics VII*, edited by D. Stauffer (World Scientific, Singapore, 2000), pp. 203–264.
 - [2] B. Drossel, *Adv. Phys.* **50**, 209 (2001).
 - [3] M. E. J. Newman and P. Sibani, *Proc. R. Soc. Lond. B* **266**, 1583 (1999).
 - [4] M. E. J. Newman and R. G. Palmer, *Modeling Extinction* (Oxford University Press, Oxford, 2003).
 - [5] S. Bornholdt, K. Sneppen, and H. Westphal, arXiv:q-bio.PE/0608033 (2006).
 - [6] J. N. Thompson, *Trends Ecol. Evol.* **13**, 329 (1998).
 - [7] J. N. Thompson, *Science* **284**, 2116 (1999).
 - [8] B. Drossel, P. G. Higgs, and A. J. McKane, *J. theor. Biol.* **208**, 91 (2001).
 - [9] T. Yoshida, L. E. Jones, S. P. Ellner, G. F. Fussmann, and N. G. Hairston, *Nature* **424**, 303 (2003).
 - [10] T. D. Kocher, *Nature Reviews. Genetics* **5**, 288 (2004).
 - [11] J. L. Crosby, *Heredity* **25**, 253 (1970).
 - [12] S. A. Kauffman and S. Johnsen, *J. theor. Biol.* **149**, 467 (1991).
 - [13] S. A. Kauffman, *The origins of order. Self-organization and selection in evolution* (Oxford University Press, Oxford, 1993).
 - [14] G. Caldarelli, P. G. Higgs, and A. J. McKane, *J. theor. Biol.* **193**, 345 (1998).
 - [15] B. Drossel, A. McKane, and C. Quince, *J. theor. Biol.* **229**, 539 (2004).
 - [16] K. Christensen, S. A. di Collobiano, M. Hall, and H. J. Jensen, *J. theor. Biol.* **216**, 73 (2002).
 - [17] M. Hall, K. Christensen, S. A. di Collobiano, and H. J. Jensen, *Phys. Rev. E* **66**, 011904 (2002).
 - [18] S. A. di Collobiano, K. Christensen, and H. J. Jensen, *J. Phys. A* **36**, 883 (2003).
 - [19] P. A. Rikvold and R. K. P. Zia, *Phys. Rev. E* **68**, 031913 (2003).
 - [20] R. K. P. Zia and P. A. Rikvold, *J. Phys. A* **37**, 5135 (2004).

- [21] V. Sevim and P. A. Rikvold, *J. Phys. A* **38**, 9475 (2005).
- [22] D. Chowdhury, D. Stauffer, and A. Kunwar, *Phys. Rev. Lett.* **90**, 068101 (2003).
- [23] D. Chowdhury and D. Stauffer, *J. Biosciences* **30**, 277 (2005).
- [24] S. Gavrillets and C. R. B. Boake, *Am. Naturalist* **152**, 706 (1998).
- [25] S. Gavrillets, H. Li, and M. D. Vose, *Evolution* **54**, 1126 (2000).
- [26] S. Gavrillets and A. Vose, *Proc. Natl. Acad. Sci. USA* **102**, 18040 (2005).
- [27] R. V. Solé, J. Bascompte, and S. Manrubia, *Proc. R. Soc. Lond. B* **263**, 1407 (1996).
- [28] P. A. Rikvold, in *Noise in Complex Systems and Stochastic Dynamics III*, edited by L. B. Kish, K. Lindenberg, and Z. Gingl (SPIE, The International Society for Optical Engineering, Bellingham, WA, 2005), pp. 148–155. E-print arXiv:q-bio.PE/0502046.
- [29] P. A. Rikvold, submitted to *J. Math. Biol.*. E-print arXiv:q-bio.PE/0508025.
- [30] K. Sato, Y. Ito, T. Yomo, and K. Kaneko, *Proc. Natl. Acad. Sci. USA* **100**, 14086 (2003).
- [31] M. Eigen, *Naturwissenschaften* **58**, 465 (1971).
- [32] M. Eigen, J. McCaskill, and P. Schuster, *J. Phys. Chem.* **92**, 6881 (1988).
- [33] S. Gavrillets, *Proc. R. Soc. Lond. B* **266**, 817 (1999).
- [34] S. Gavrillets, *Fitness landscapes and the origin of species* (Princeton University Press, Princeton and Oxford, 2004).
- [35] P. F. Verhulst, *Corres. Math. et Physique* **10**, 113 (1838).
- [36] J. D. Murray, *Mathematical Biology* (Springer-Verlag, Berlin, 1989).
- [37] A. Roberts, *Nature (London)* **251**, 607 (1974).
- [38] G. Hardin, *Science* **131**, 1292 (1960).
- [39] R. A. Armstrong and R. McGehee, *Am. Naturalist* **115**, 151 (1980).
- [40] P. J. den Boer, *Trends Ecol. Evol.* **1**, 25 (1986).
- [41] S. P. Hubbell, *The Unified Neutral Theory of Biodiversity and Biogeography* (Princeton University Press, Princeton, 2001).
- [42] J. A. J. Metz, R. M. Nisbet, and S. A. H. Geritz, *Trends Ecol. Evol.* **7**, 198 (1992).
- [43] M. Doebeli and U. Dieckmann, *Am. Naturalist* **156**, S77 (2000), and references therein.
- [44] C. J. Krebs, *Ecological Methodology* (Harper & Row, New York, 1989), Chap. 10.
- [45] N. Eldredge and S. J. Gould, in *Models In Paleobiology*, edited by T. J. M. Schopf (Freeman, Cooper, San Francisco, 1972), pp. 82–115.
- [46] S. J. Gould and N. Eldredge, *Paleobiology* **3**, 115 (1977).
- [47] S. J. Gould and N. Eldredge, *Nature (London)* **366**, 223 (1993).
- [48] P. A. Rikvold, submitted to *Int. J. Mod. Phys. C*. E-print arXiv:q-bio.PE/060913.
- [49] M. Paczuski, S. Maslov, and P. Bak, *Phys. Rev. E* **53**, 414 (1996).
- [50] S. N. Dorogovtsev, J. F. F. Mendes, and Y. G. Pogorelov, *Phys. Rev. E* **62**, 295 (2000).